

Understanding the prompt events in $\pi^+ \rightarrow e^+\nu$ and $\pi^+ \rightarrow e^+\nu\gamma$ DST.

Maxim A. Bychkov

02 May 2006

Version 1.1

1 Introduction

Prompt events generated by the interactions of the beam particles with the beam detectors material have been our main tool to identifying the zero time of an event in the PIBETA data analyzes. All of the strong interactions of the beam particles are nearly instantaneous for our detector. By observing the products of such interactions and knowing the arrival time of the beam we can tie an event to an absolute time reference. The separation between the accelerator bunches is known to a very high degree of accuracy and is used as a clock to fix the events occurring in the PIBETA detector in the laboratory time frame.

Traditionally the analyzes proceeds as follows. After generating a DST for a given reaction such as $\pi^+ \rightarrow e^+\nu$ or $\pi^+ \rightarrow e^+\nu\gamma$, prompt events are separated from the rest of the events. It can be accomplished by various means.

One method is based on the fact that prompt events are the result of the beam particle interacting early in the degrader or the target thus depositing most of its kinetic energy in these beam detectors. On the contrary, the decays of the beam particles at rest are followed by the emission of the secondary particles which carry portion of the particle's energy to be later deposited in the CSI calorimeter. This is well illustrated in fig. 1, where the energy in the degrader is plotted against the event time for all the events

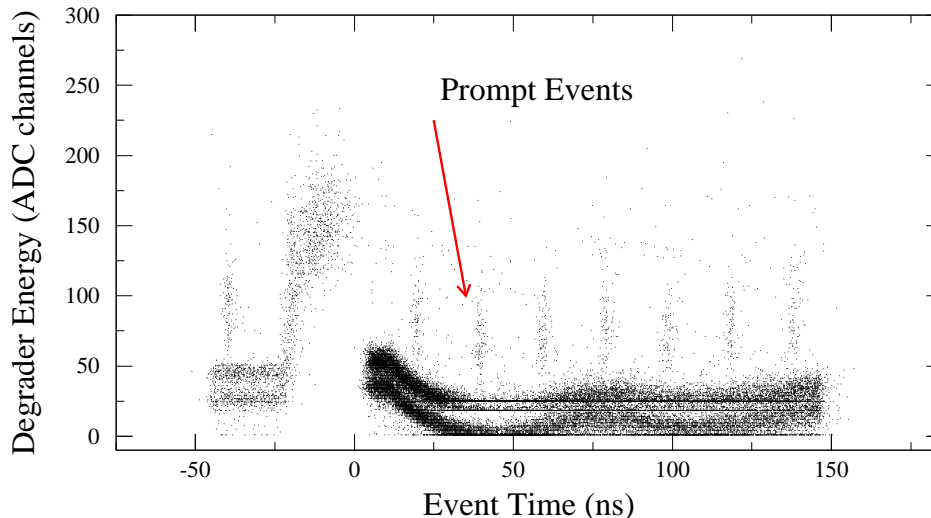


Figure 1: Degraded energy vs. event time for all events in the $\pi^+ \rightarrow e^+\nu$ DST. Prompt events which are in time with the beam particles deposit more energy in the degrader.

in a small sample of the $\pi^+ \rightarrow e^+\nu$ DST. We can clearly identify two distinct regions on the plot. The events with higher energy deposition have a characteristic prompt time structure.

The second method is based on the fact that if a particle interacts in the degrader, it does not produce the pi-stop signal, i.e., there will be an uncorrelated number of hits in the beam counters. We can then extract from the DST the events which have hits in the B0 counter and the degrader but do not have correlated hits in the target (or alternatively no corresponding pi-stop signal). It is parametrized the following way.

$$|t_{\text{B0}} - t_{\text{degr}}| > 7 \text{ or } |t_{\text{B0}} - t_{\text{target}}| > 7$$

After applying any of the cuts described above (or the combination of two) the resulting time spectrum looks as shown in fig. 2.

The positions of the prompt peaks are fit with an appropriate function (a Gaussian around the peak or a Gaussian plus an exponent in a wider range) and the results of the measurement are fit with a linear function of the multiple of the cyclotron frequency (beam bunches separation time). The linear fit provides us with a time offset of a sample. The high statistics $\pi^+ \rightarrow e^+\nu$ DST yields the most accurate results which are subsequently used

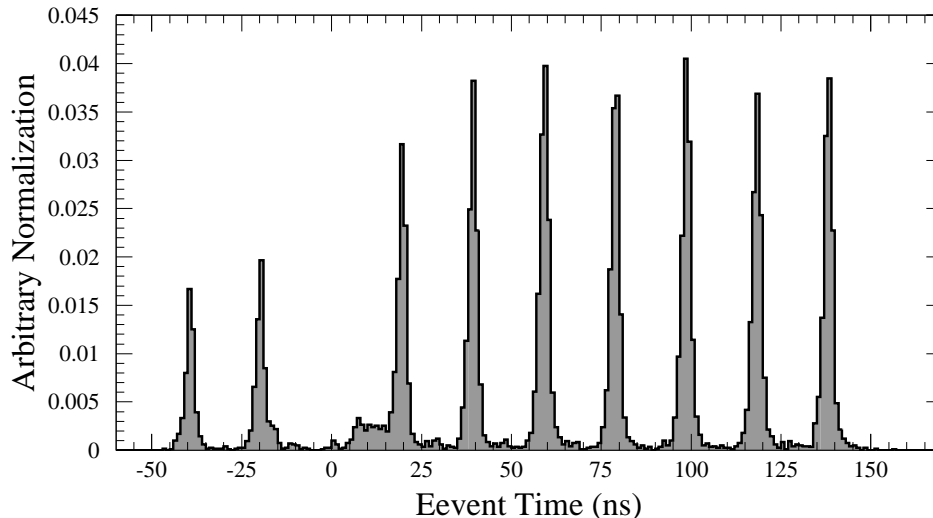


Figure 2: Event time for the prompt events in the $\pi^+ \rightarrow e^+\nu$ DST.

to offset all of the data in a given 1H trigger.

2 Stating the problem

Fig. 3 shows a subset of the prompt peaks for the $\pi^+ \rightarrow e^+\nu$ and $\pi^+ \rightarrow e^+\nu\gamma$ DST simultaneously. Two DSTs are corrected by the same common offsets determined from the $\pi^+ \rightarrow e^+\nu$ DST.

It is clear that the positions of the $\pi e2$ prompt peak are properly positioned at the multiple of the cyclotron frequency of 19.75 ns while the prompt peaks in $\pi e2\gamma$ are systematically shifted to an earlier time. On the other hand fig. 4 shows all of the events in both DSTs within the pion gate. The beginning and the end of the gates appear to be lined up reasonably well.

One explanation can be that the prompt events in the $\pi e2$ DST are physically different than the prompt events in the $\pi e2\gamma$ DST. The following set of figures 5 – 8 demonstrates various physical distributions for the prompt events in two different DST. It is, indeed, obvious that the physical processes passing the prompt cuts are drastically different.

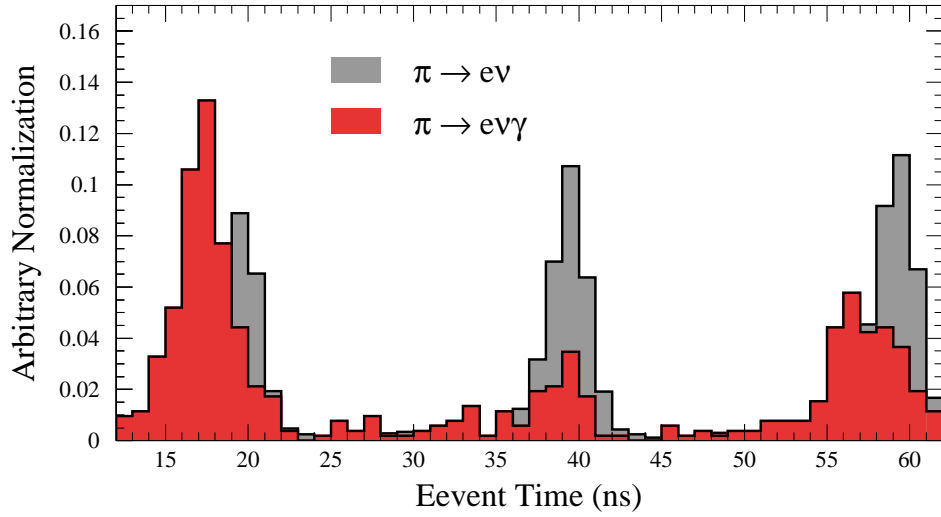


Figure 3: Event time for the prompt events in the $\pi e2$ and $\pi e2\gamma$ DSTs.

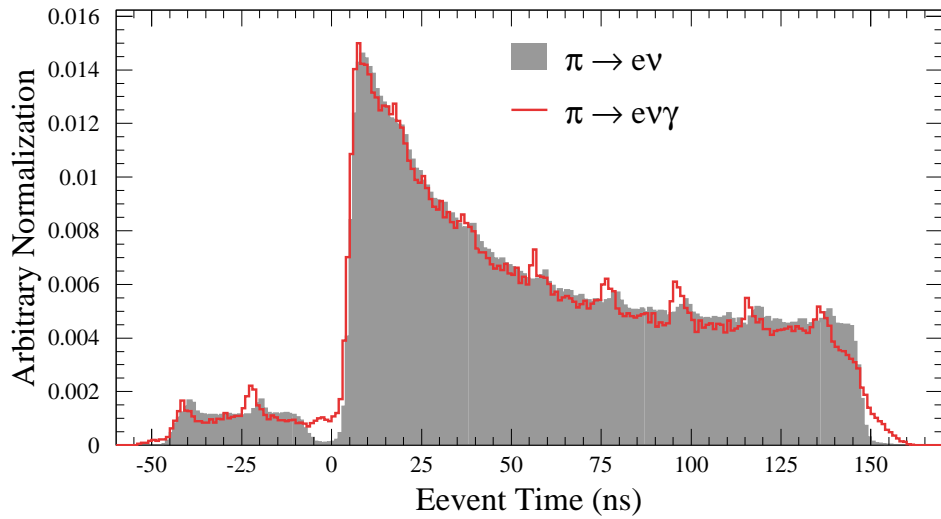


Figure 4: Event time for all events in the $\pi e2$ and $\pi e2\gamma$ DSTs within an entire pion gate.

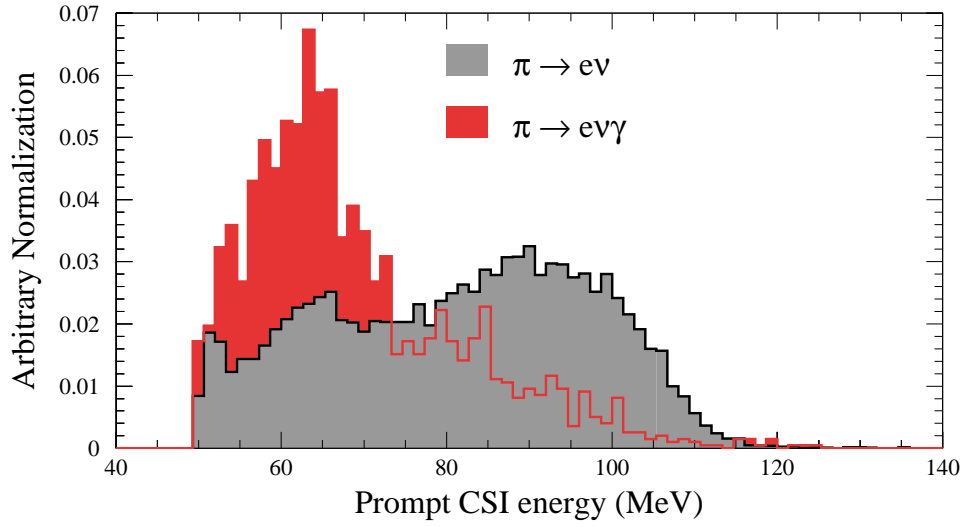


Figure 5: Energy in CsI for prompt events in the $\pi e2$ and $\pi e2\gamma$ DSTs.

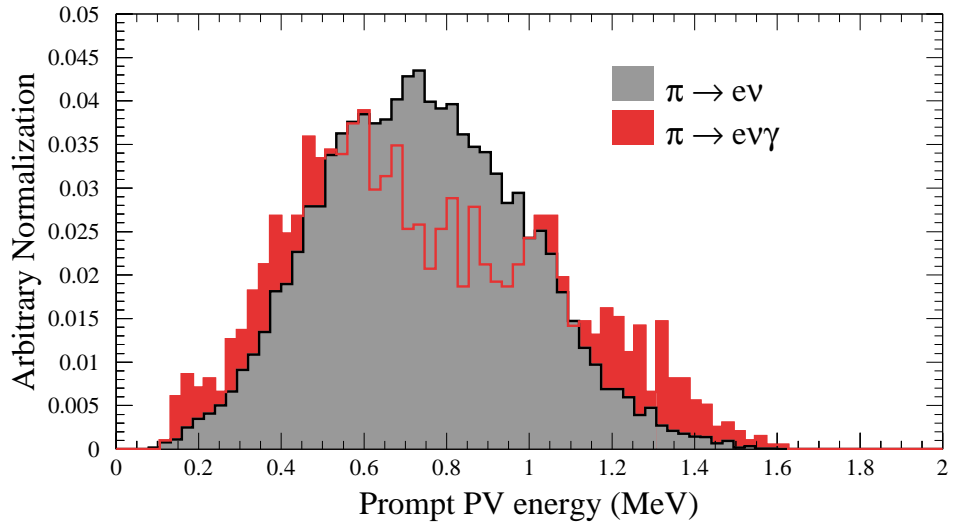


Figure 6: Energy in PV for prompt events in the $\pi e2$ and $\pi e2\gamma$ DSTs.

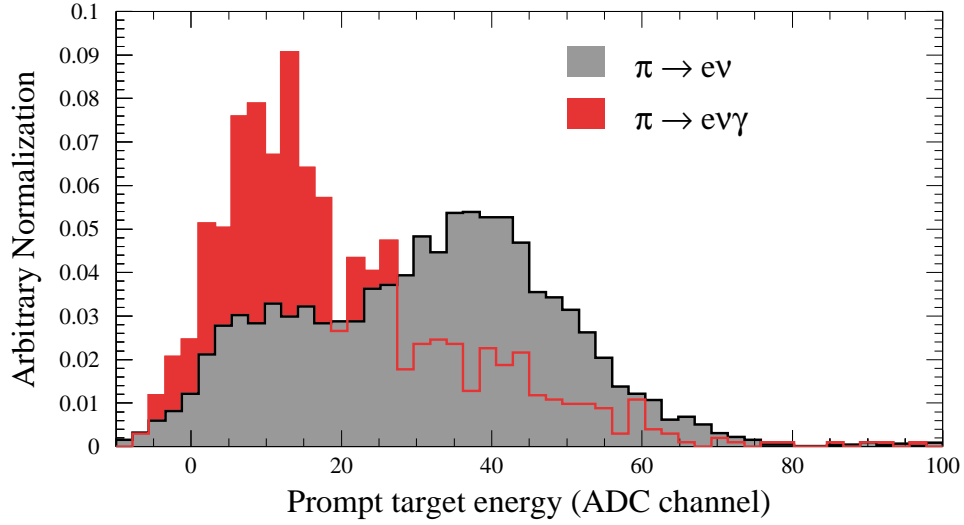


Figure 7: Energy in the target for prompt events in the $\pi e2$ and $\pi e2\gamma$ DSTs.

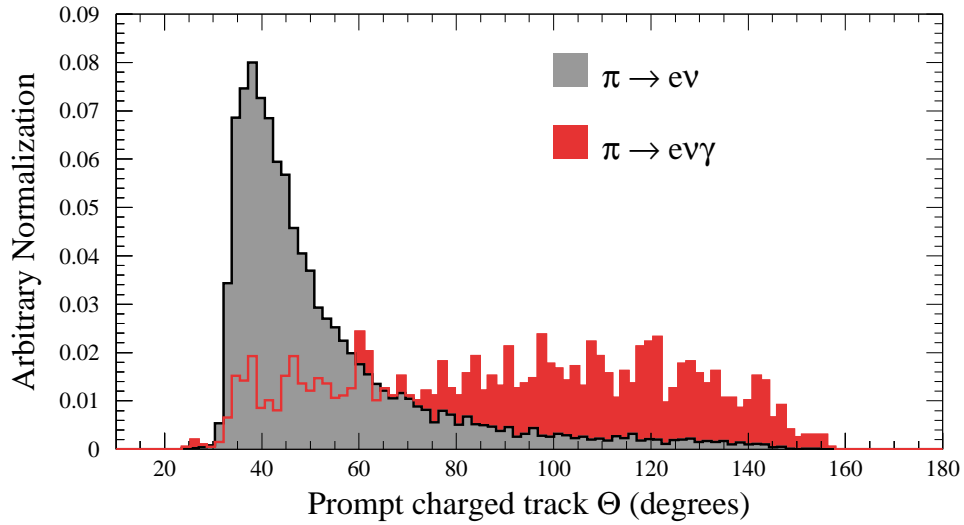


Figure 8: Charged track θ angular distribution for prompt events in the $\pi e2$ and $\pi e2\gamma$ DSTs.

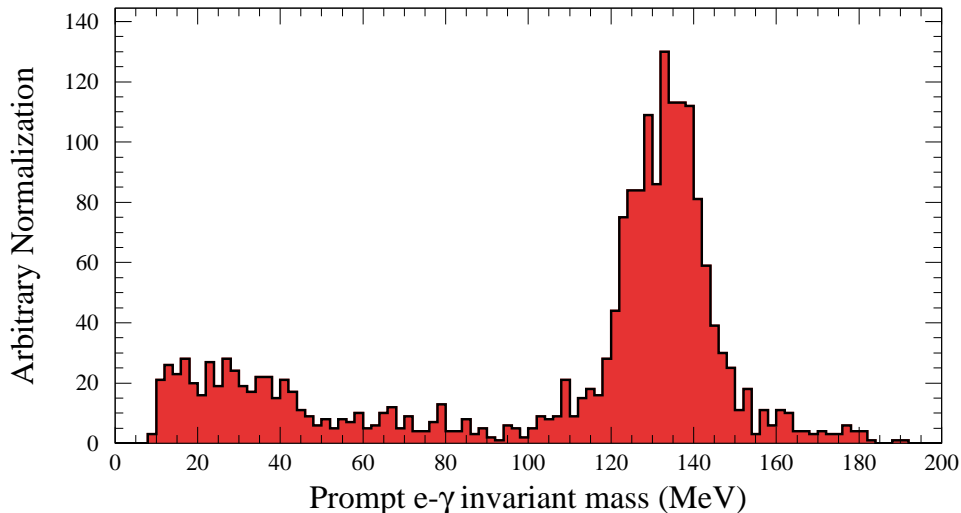


Figure 9: The invariant mass of the prompt positron-photon pair in $\pi e 2\gamma$ DST.

3 Problem solution

We are facing the problem of identifying what types of particles contribute to the prompt events in either data sample. $\pi e 2\gamma$ sample gives us a clearer picture once we plot the invariant mass of the prompt positron-photon pair as shown in fig. 9. We can identify a monochromatic peak around 140 MeV which corresponds to the mass of π^0 .

Fig. 10 shows that the energy spectrum of the prompt gamma for the same data set is dominated by the peak at 70 MeV. In addition fig. 11 demonstrates that the opening angle between the positron and the photon is large while the true $\pi e 2\gamma$ events are dominated by the inner bremsstrahlung photons with small opening angles. Finally fig. 12 shows the position of the charged track projected to the detector z -axis. Most of the prompt events come from the degrader. It is when the incoming π^+ has enough energy to undergo the SCX reaction. This type of events are, perhaps, the following chain of prompt events in the degrader:

$$\pi^+ A \rightarrow B \pi^0$$

subsequently

$$\pi^0 \rightarrow \gamma \gamma^* \rightarrow \gamma e^+ e^-$$

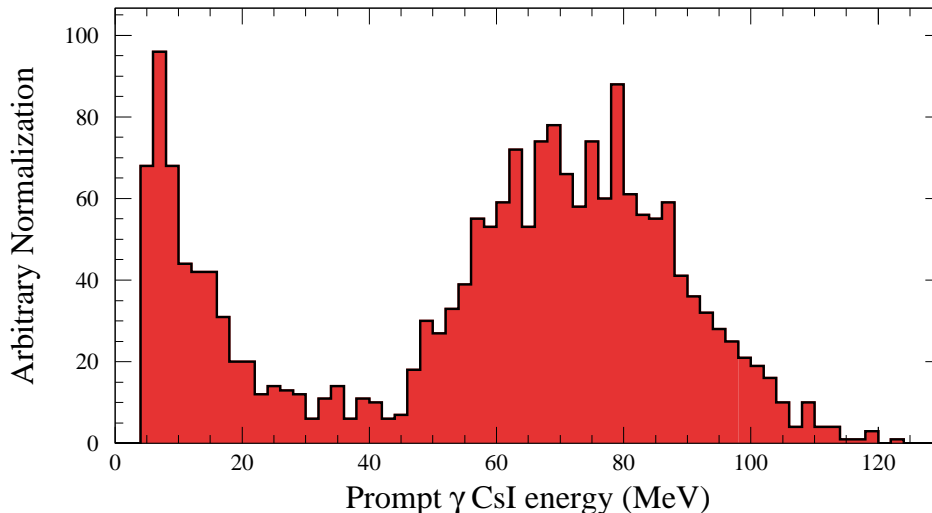


Figure 10: The energy deposited by prompt photon in CsI calorimeter in $\pi e 2\gamma$ DST.

where A and B are the degrader/target nuclei and conversion of the γ^* to a e^+e^- pair could be Dalitz or in the material.

The remaining prompt events with the invariant mass below 100 MeV can be attributed to the accidental coincidental background of $\pi e 2$ events with the split clumps in the calorimeter. It is confirmed by the distribution of the charged track vertex for these events shown in fig. 13 which correspond to the actual pion stop distribution. Fig. 14 demonstrates strong correlation between the positron and photon energies for the events with invariant mass below 100 MeV.

The situation with the prompt events in the $\pi e 2$ DST is more difficult. As seen in fig. 5 the energy spectrum of these events is dominated by the particles identified as positrons but with energies above 70 MeV. Neither decays of the π^0 into photons nor accidental coincidence of the $\pi^+ \rightarrow e^+\nu$ positron with a stray photon can produce such energetic spectra. Fig. 6 rules out the possibility of the protons emitted in the SCX reaction since the PV energy for the protons is significantly higher than for positrons.

Another measurement rules out protons. Unlike positrons, protons do not create electro-magnetic showers in the CsI calorimeters. Therefore, if hit centrally, a single crystal contains nearly 100% of the deposited energy. Positron induced showers, however, spread to the neighboring crystals even

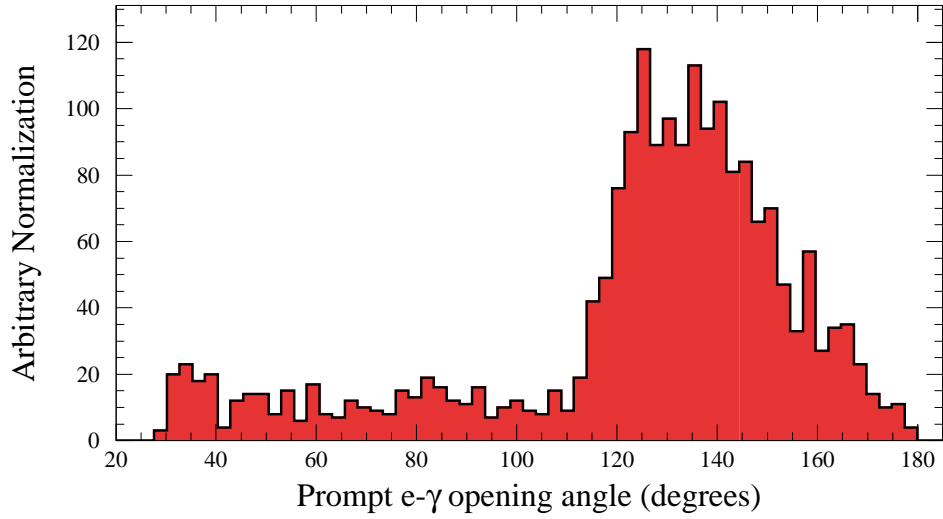


Figure 11: The prompt positron-photon pair opening angle in $\pi e2\gamma$ DST.

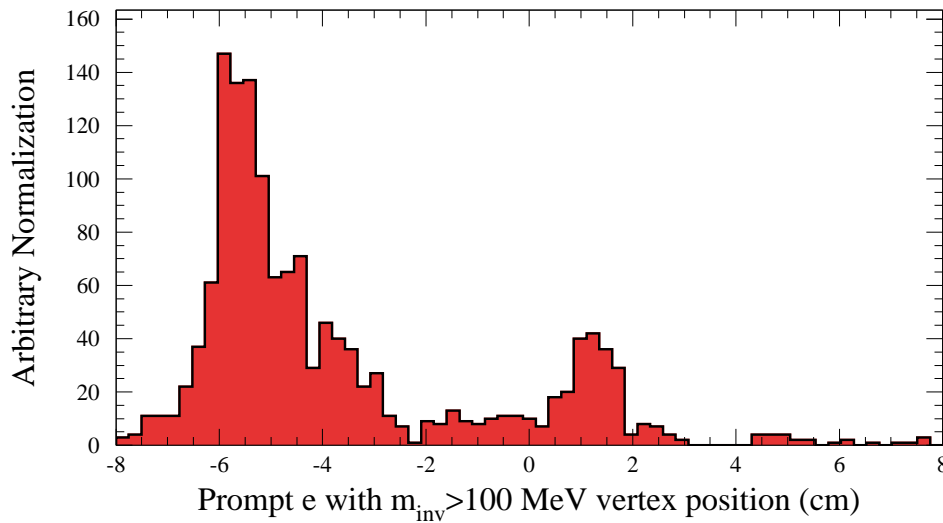


Figure 12: Prompt positron trajectory projected to the z -axis of the detector in $\pi e2\gamma$ DST for the events with high invariant mass.

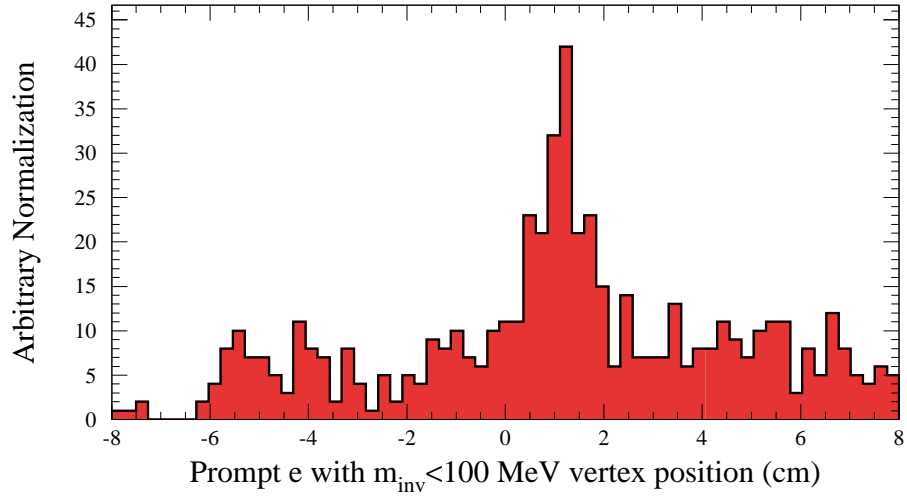


Figure 13: Prompt positron trajectory projected to the z -axis of the detector in $\pi e 2\gamma$ DST for the events with low invariant mass.

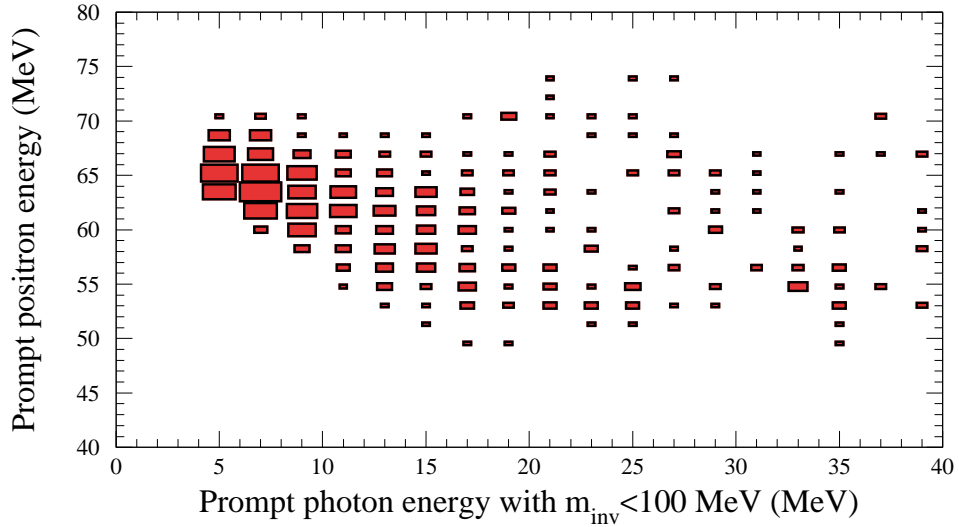


Figure 14: Prompt positron energy vs. prompt photon energy in $\pi e 2\gamma$ DST for the events with low invariant mass.

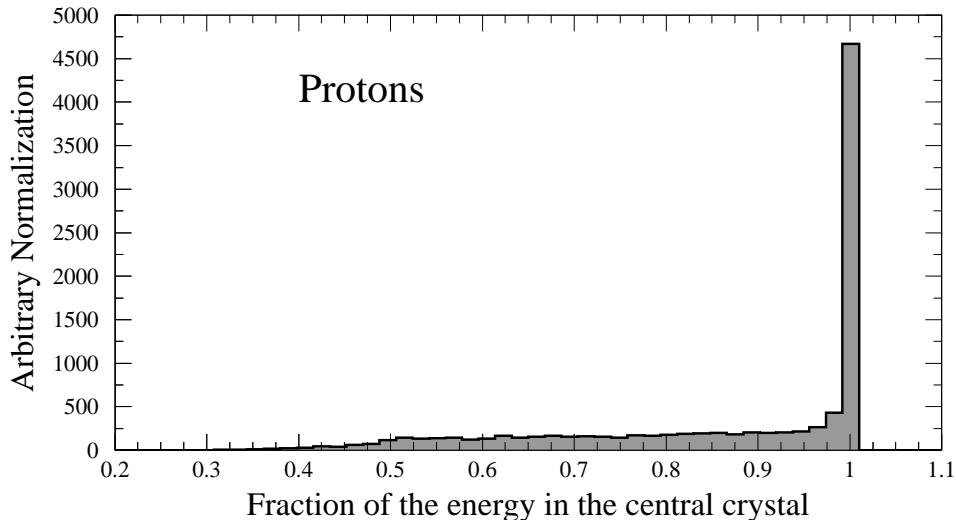


Figure 15: Fraction of the energy in the central crystal to the total clump energy for the clean sample of protons in $\pi e2$.

in case of the central hit. Fig. 15 and fig. 16 show the ratio of the energy in the central crystal to the total energy in the clump for clearly identified protons and positrons respectively. The following criteria are used to separate protons and positrons in the $\pi e2$ DST.

$$\begin{aligned} \text{proton} & \quad E_{PV} > 3.6 \cdot \exp(-0.007(E_{CsI} + E_{PV})) \\ \text{positron} & \quad 0.2 \cdot \exp(-0.007(E_{CsI} + E_{PV})) < E_{PV} < 3.6 \cdot \exp(-0.007(E_{CsI} + E_{PV})) \end{aligned}$$

additionally for positrons

$$E_{CsI}^{\text{positron}} < 80 \text{ MeV}$$

For all particles we require a central hit, i.e., the angle between the charged track and the center of the crystal $\theta < 5^\circ$.

Applying the same technique to the particles in question we obtain the plot shown in fig. 17 which is very indicative of the positrons.

Once established that the unknown particles are positrons, we are left with only two possibilities. First is that the high energy positrons are caused by the positron pile up, i.e., two random positrons end up in the same clump and deposit significant amount of energy. We should bear in mind that at

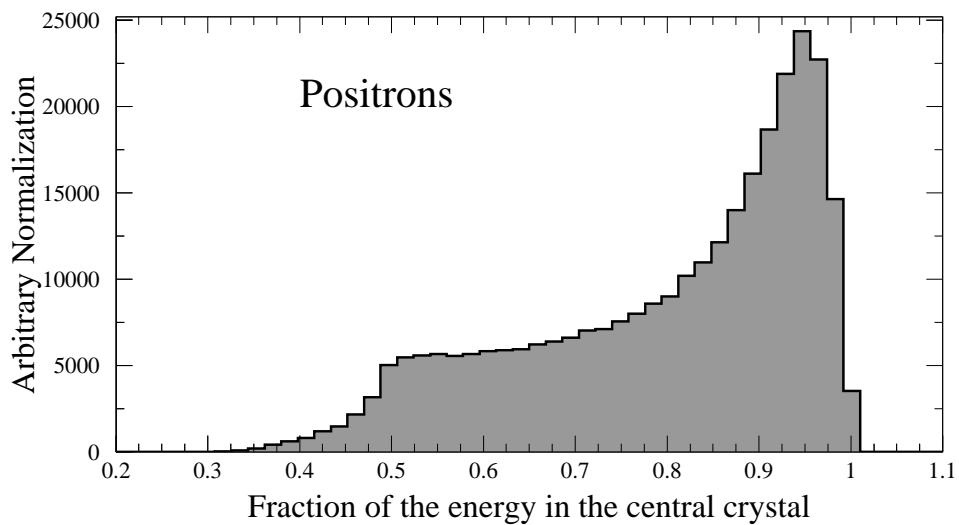


Figure 16: Fraction of the energy in the central crystal to the total clump energy for the clean sample of positrons in $\pi e2$.

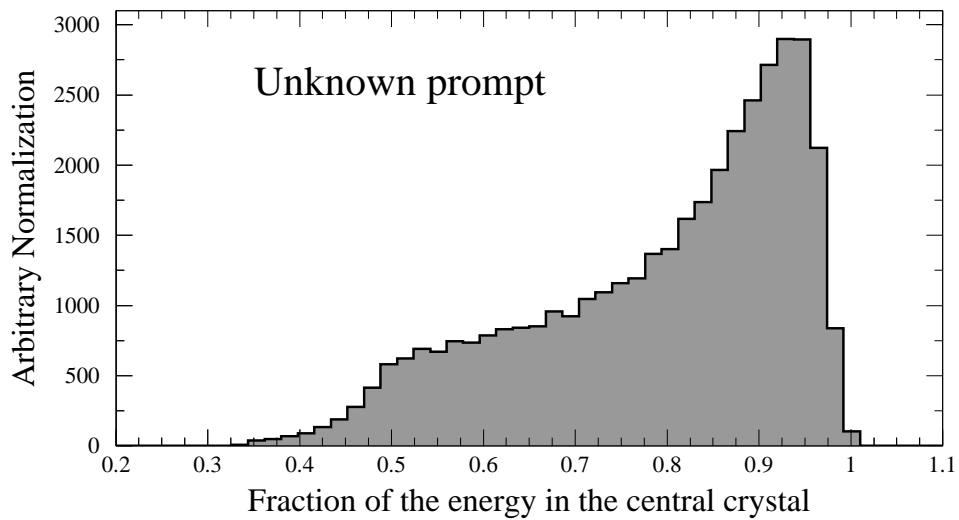


Figure 17: Fraction of the energy in the central crystal to the total clump energy for the unknown prompt events in $\pi e2$.

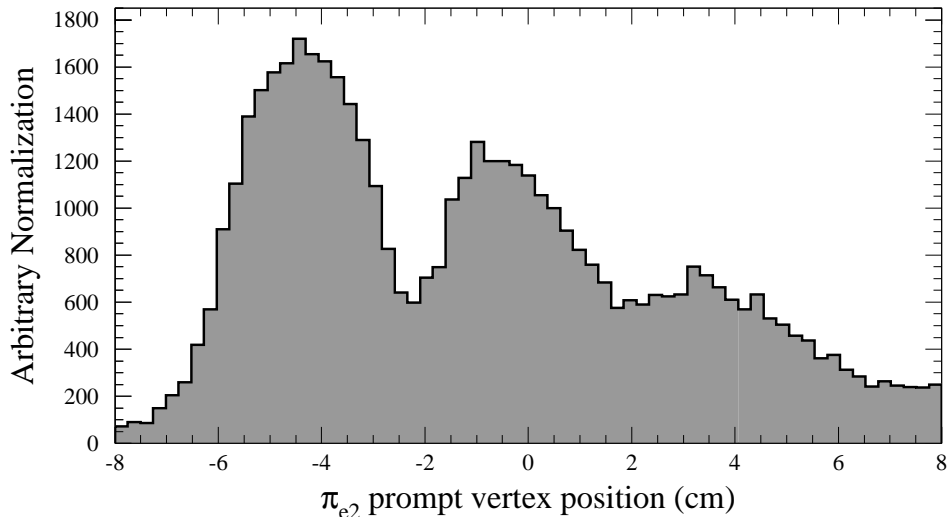


Figure 18: Prompt positron trajectory projected to the z -axis of the detector in $\pi e2$ DST.

least one of the positrons should fire a 1H trigger. In such a case the BR of such events is strongly rate dependent. We analyzed two sets of runs with the pi-stop rates of 130 KHz and 50 KHz respectively. The total number of pi-stops for each set is $2.98 \cdot 10^9$ and $2.90 \cdot 10^9$ which makes it rate independent. The total number of high energy positrons observed for the identical set of cuts is $3.2 \cdot 10^3$ and $3.0 \cdot 10^3$ respectively. There are several additional indications that these events are not the positron pile-up. For once, it will not explain the observed time shift compared to the $\pi e2\gamma$ prompts. Secondly, the distribution of the positron vertex along the z -axis shown in fig. 18 is typical of the true prompt events, while the pile up positrons are coming predominantly from the target.

The remaining possibility is the beam positrons scattered in the degrader/target material. Although seemingly an exotic possibility, it renders a second look. Beam positrons at given momenta of 113–116 MeV/c are highly relativistic and travel much faster than beam pions and muons. As can be seen in fig. 19 for the given base length of ~ 21 m positrons from completely different beam bunches can come in very close proximity to the original pions, thus explaining the systematic time shift of our prompt particles. Moreover, only beam positrons scattered elastically have enough energy to be qualified and they can scatter pretty much uniformly throughout the beam elements

(fig. 18) and exclusively into the forward angles (fig. 8).

Fig. 20–23 show the GEANT3 simulation of the beam positrons with 113 MeV/c momentum. Even though the simulation does not reproduce all the aspects faithfully, there can be little doubt that the high energy particles in the $\pi e2$ DST are indeed the scattered beam positrons. It is worth mentioning that if the time offsets from the $\pi e2$ DST are kept it will not affect the $\pi^+ \rightarrow e^+\nu\gamma$ results since it is normalized to $\pi^+ \rightarrow e^+\nu$ events as long as both processes are observed in the same gate. It will, however, modify the absolute BR of the $\pi^+ \rightarrow e^+\nu$ by the factor of $\exp(\Delta t/\tau_\pi)$ with Δt the amount of the delay of the prompt positrons with respect to true pion induced prompts.

Path length 20.7m

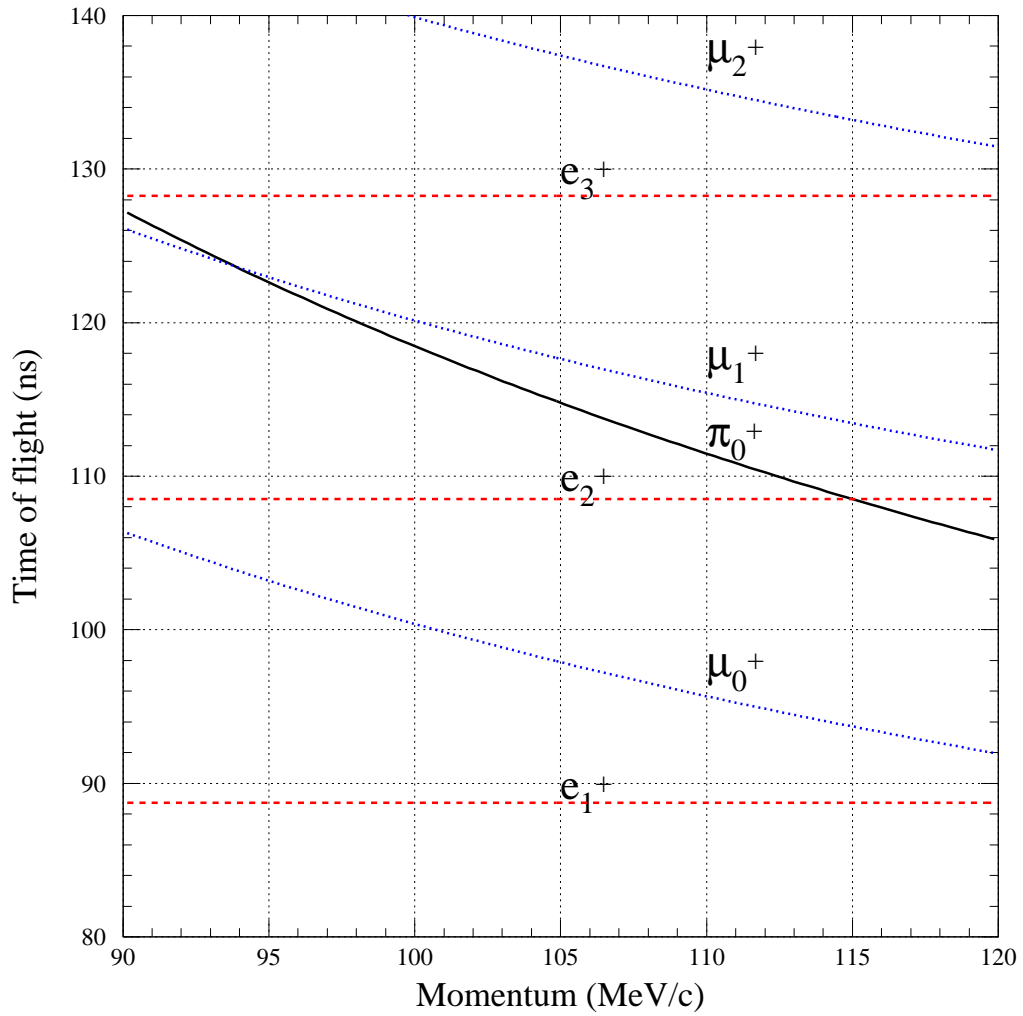


Figure 19: Time of flight as a function of the particle's momentum for different types of particles in the beam.

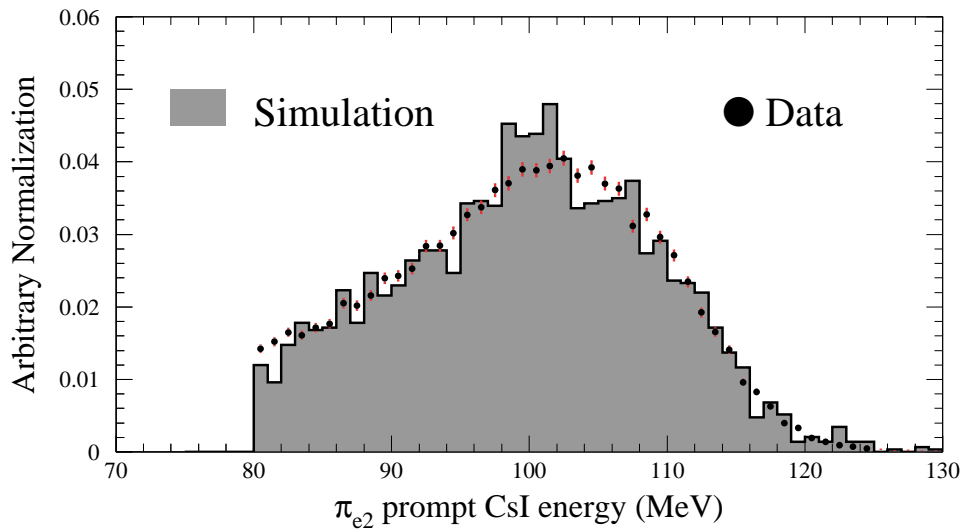


Figure 20: Energy in the CsI deposited by the beam positrons. Solid area represents simulation and dots are data.

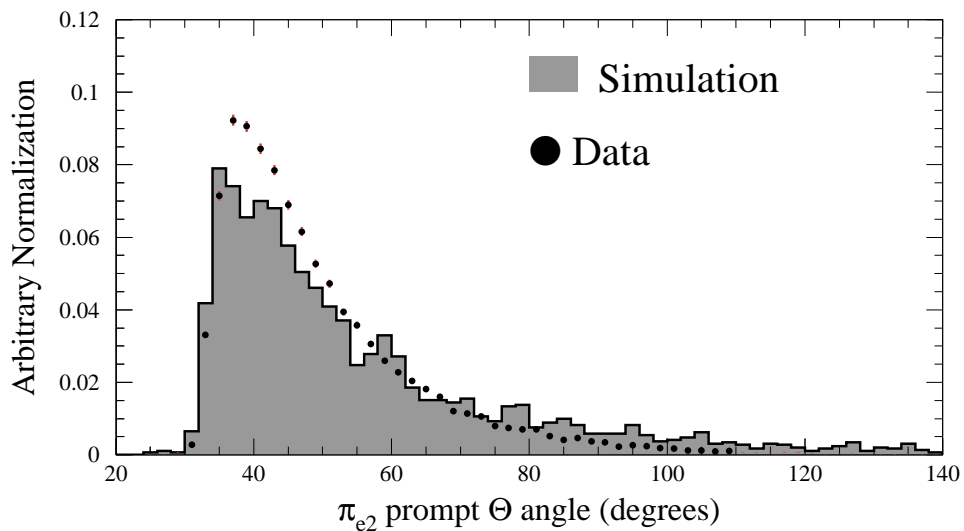


Figure 21: Track angle with the direction of the beam for scattered beam positrons. Solid area represents simulation and dots are data.

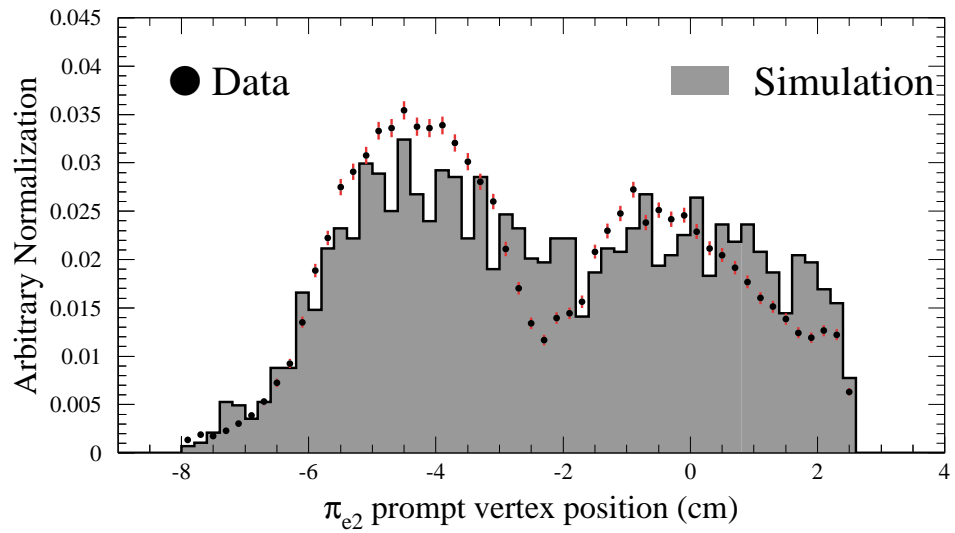


Figure 22: Prompt scattered positron trajectory projected to the z -axis of the detector. Solid area represents simulation and dots are data.

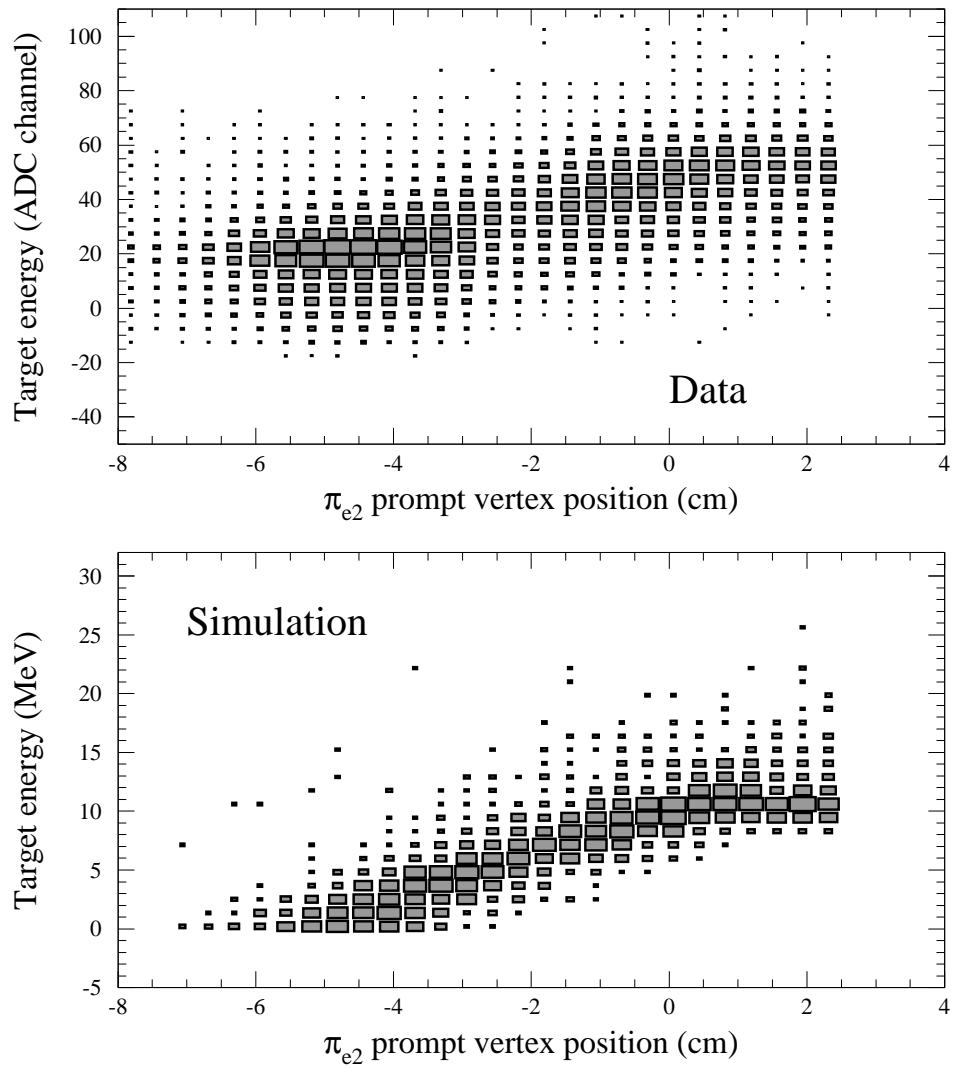


Figure 23: Energy in the target vs. track projection for the beam scattered positrons.